

Dissipationless tune-out trapping for a lanthanide-alkali quantum gas mixture

Alexandre De Martino,^{1,*} Florian Kiesel,^{1,*} Jonas Auch,¹ Kirill Karpov,¹ and Christian Gross^{2,†}

¹*Physikalisches Institut, Eberhard Karls Universität Tübingen, 72076 Tübingen, Germany*

²*Physikalisches Institut and Center for Integrated Quantum Science and Technology,
Eberhard Karls Universität Tübingen, 72076 Tübingen, Germany*

(Dated: June 15, 2025)

Quantum gas mixtures offer a wide field of research, ranging from few-body physics of impurities to many-body physics with emergent long-range interactions and ultracold molecular gases. Achieving precision control of mixtures is much harder than for single-component gases and, consequently, the respective techniques are less developed. Here we report on a decisive step forward in this direction by realizing dissipationless and fully differential optical control of the motional degrees of freedom of one of the species without affecting the other. This is achieved in a novel Bose-Fermi mixture with extreme mass imbalance, erbium-166 and lithium-6. Our experiments pave the way to a new generation of precision many-body experiments with quantum gas mixtures with unprecedented long lifetimes and low temperatures.

Ultracold quantum gas mixtures provide a unique platform to explore heterogeneous quantum many-body systems [1]. They have been successfully used to study ultracold molecular [2, 3], polaronic [4, 5] and few-body [6] physics or to realize many-body systems with new forms of emergent interactions [7–9]. A ubiquitous difficulty for precision experiments with such mixtures is to realize dissipationless independent control of the motional degree of freedom of the involved atomic species. In principle, independent control can be achieved with lasers at particular species-dependent wavelengths, so called tune-out wavelengths. At these wavelengths, the optical polarizability of one of the species vanishes [10, 11]. Tune-out wavelengths have been measured and used in many experiments with various atomic species [12–27], and heteronuclear mixtures [11, 28–30]. Specifically for mixtures, all systems realized so far suffer from a central issue: the tune-out wavelengths emerge due to destructive interference of the polarizability contribution of atomic transitions, which are not far detuned enough to prevent excess heating of at least one of the species due to photon scattering. In a tune-out trapped mixture, the relevant parameter to measure the impact of dissipation is γ/U the photon scattering rate of both partners γ normalized to the potential experienced by the trapped species U . In previously reported experiments the tune-out was realized in alkalis, either in-between the D-lines with Rb-K [11] and Cs-Li [30], or using the blue lines to cancel the polarizability in Rb-Yb [28]. In all these mixtures, γ/U is at least one order of magnitude larger than usually achieved in single species experiments. In contrast, the lanthanide elements feature very narrow and closed transitions lines far in the infrared, ideal to realize dissipationless differential control when combined with alkali atoms.

Here we report on the measurement of a tune-out wavelength for ^{166}Er near its 841 nm-line (see Fig. 1) which we combine with ^6Li in our dual-species experiment. We observe very low dissipation for both Er and Li, as expected

for the large effective detuning of the tune-out wavelength to all transitions. We precisely determine the dependence of the tune-out wavelength on the relative angle between polarization and magnetic field. This provides accurate spectroscopic data for the tensor light shift in Er, which significantly deviates from the predictions based on the line data published in [31]. Our experiments pave the way for a new generation of dual species precision experiments with fully differential control over the motional degrees of freedom. This allows for the experimental study of motional properties of impurities with extreme mass imbalance [32], the implementation of novel sympathetic cooling schemes to achieve lower reduced temperatures for ultracold fermions [33, 34], and the study of fermionic lattice systems in contact with a bosonic bath [35, 36].

Our experiment features spatially separated magneto-optical traps for Er and Li, which are placed in line of sight with each other and a glass cell providing high optical access. Both gases are transported into this cell in a running optical lattice realized with 1064 nm laser light. Li is transported over a distance of 1 m, Er over 0.5 m using two Gaussian beams with displaced foci [37]. Additionally, Er is magnetically levitated against gravity during transport. In all measurements reported here, we either work with Er or with Li, loaded into orthogonally crossed single-mode laser beams with beam waists of $35\,\mu\text{m} \times 580\,\mu\text{m}$ at 1064 nm after transport. This provides a trap with a depth of $36\,\mu\text{K}$ for Li and $15\,\mu\text{K}$ for Er. The large aspect ratio is required to prevent heating during loading from the lattice and to confine Er against gravity. A vertical magnetic field of a few Gauss is used to conserve the spin alignment of the gases. For a more detailed experimental description, see the Supplemental Material [38] (see also references [39–42] therein). We superimpose a smaller dimple laser beam at 841 nm derived from a titanium-sapphire laser with waists of $6\,\mu\text{m} \times 28\,\mu\text{m}$ and with a power of up to 0.5 W. This beam propagates in a direction perpendicular to the magnetic field, and its polarization is precisely aligned to be linear

with an angle $\theta = 90^\circ$ to it. The laser is frequency stabilized to a low-drift reference cavity and tunable over a range of several 100 GHz with negligible frequency-error in this range.

The size of the dimple is chosen such that for the same atom numbers, a degenerate Fermi gas of Li trapped in it is fully immersed in a Bose-Einstein condensate of Er held in the large 1064 nm trap. The separation of scales, even more in single particle eigenenergies than in trap size, is advantageous: the dimple trap realizes a tune-out for Er only, but Li, being much more tightly trapped, is essentially unaffected by the small gradients of the large trap. A separation of scales is present in many properties of our Er-Li mixture. In contrast to Li, Er is very heavy and magnetic. Li features few very broad Feshbach resonances [43], while Er has many much narrower ones [44] and also first studies of interspecies resonances have been reported [45]. This is an ideal starting point to explore optimized sympathetic cooling of the fermions with a largely populated coolant, that can initially be prepared below one-hundreds of the fermi temperature [46]. Recent experiments with a similarly mass-imbalance Dy-Li mixture [47] and a dual Bose gas of Er-Li [48] have already demonstrated thermalization between the two components.

To measure the tune-out wavelength, we modulate the power of the dimple beam with 100% amplitude-variation and variable frequency (see Fig. 1). After about 1 s of modulation we measure the remaining atom number. Without fine-tuning of the dimple wavelength we observe several resonances corresponding to the trap frequency in the 1064 nm dipole trap and its harmonics. In contrast, no effect of the modulation is visible when the dimple trap wavelength is set to the tune-out value. To precisely locate it relative to the $\Gamma_{841}^{(\text{Er})} = 2\pi \times 8 \text{ kHz}$ wide transition at 841.22 nm, we measure the remaining atom number versus the detuning $\Delta_{841}^{(\text{Er})}$. A Gaussian fit to the data reveals the tune-out point for this geometry at $\delta_{90^\circ} = 244 \pm 1 \text{ GHz}$ and we experimentally confirmed that the results are independent of the intensity of the 1064 nm trap. The found tune-out frequency is far blue detuned $\delta_{90^\circ} \approx 3.1 \cdot 10^7 \Gamma_{841}^{(\text{Er})}$ to the 841 nm-line of Er.

To quantify the dissipative effect of the laser light at the tune-out wavelength due to photon scattering, we measure the lifetime of Er in the 1064 nm trap while exposed to the dimple light. We set the dimple power to 0.5 W, which corresponds to a trap depth for Li of $U^{(\text{Li})} = k_B \cdot 0.2 \text{ mK}$. The measured lifetimes, shown in Fig. 2, demonstrate the non-dissipative character of our dimple trap for Er. For holding times up to 100 s, we do not observe any detectable change of the $1/e$ -lifetime. We measure $\tau_{841}^{(\text{Er})} = 64 \pm 5 \text{ s}$ with and $\tau^{(\text{Er})} = 58 \pm 6 \text{ s}$ without dimple. Our observation matches the theoretical prediction: photon scattering with rate γ transmits energy to the trapped gas according to $\dot{E} = 2E_r\gamma$,

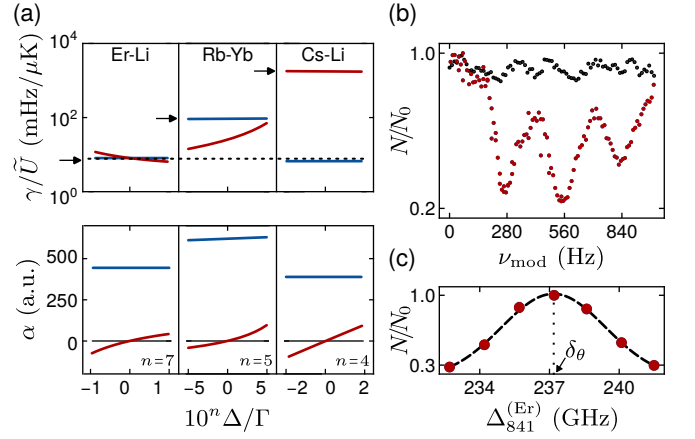


Figure 1. System comparison and tune-out spectroscopy. (a) We compare three mixtures, for which tune-out trapping has been realized regarding their normalized photon scattering γ/\tilde{U} (top) and their polarizabilities α in atomic units (a.u.) (bottom). The normalization by $\tilde{U} = U/k_B$, with k_B being Boltzmann's constant, is done with regard to the potential U seen by the trapped species. The arrows in the top panel indicate the relevant value dominated by the most dissipative partner, and the dashed line is a reference value for the often realized single species configuration: Rb trapped in 1064 nm light. In both panels, the red lines indicate the tuned-out element (Er, Rb, Cs), the blue lines the trapped partners (Li, Yb, Li). The horizontal axis displays the normalized and scaled detuning $10^n \Delta/\Gamma$, where Δ is the frequency difference to the tune-out point (for Er: 841 nm, Rb: 423 nm, Cs: 880 nm), Γ is the line width of the nearest transition line of the tuned-out element and n accounts for the different distance of this line to the tune-out point. (b) Trap-loss spectrum of Er in the 1064 nm optical trap beam, which is superimposed with a 841 nm dimple beam. The intensity of the dimple beam is amplitude-modulated at different frequencies ν_{mod} . The red data is representative for a non-fine-tuned dimple wavelength away from the tune-out, the black data is on the tune-out. We attribute the slight modulation of the black data to experimental instabilities during the measurement. (c) Remaining normalized Er atom number (red dots) for resonant modulation at the frequency of the first minimum in (b) for different dimple beam detunings from the 841 nm line. Error bars of one standard deviation are smaller than the marker size. A Gaussian fit (dashed line) is used to extract the tune-out wavelength δ_θ and its uncertainty. We use the polarizability of Li and Cs from [49].

where $E_r = (\hbar k)^2/2m$ is the recoil energy imparted on the atoms of mass m from the scattered photons with wave number k . The photon scattering rate for a laser of angular frequency ω_L follows as the sum over the contributions from all far-detuned transition lines $\gamma = \sum_i \Gamma_i \Omega_i^2 / 4\Delta_i^2$ with Rabi frequency Ω_i , detuning $\Delta_i = \omega_L - \omega_i$ and inverse lifetime Γ_i of transition line i . We overestimate the scattering rate by assuming a homogeneous dimple peak intensity over the entire Er cloud and obtain a scattering rate of $\gamma^{(\text{Er})} = 1.5 \text{ Hz}$, corresponding to an energy increase rate of $\dot{E}^{(\text{Er})} =$

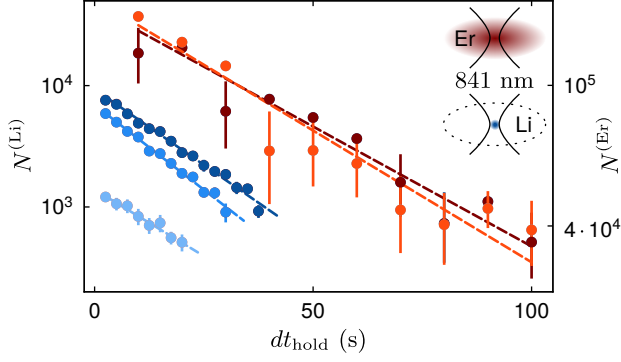


Figure 2. Dissipative effects of the tune-out beam on Er and Li. Lifetime measurements of Er in the 1064 nm optical dipole trap are shown for the 841 nm dimple beam set to the tune-out wavelength at full (dark red) and zero power (light red). The right vertical axis gives the trapped Erbium atom number $N^{(\text{Er})}$ versus holding time dt_{hold} . Each data point is averaged over five experimental repetitions. Lifetimes are extracted by an exponential fit (dashed lines) to the data. In blue, we show lifetime measurements of Li in the same dimple beam for three powers: (0.1, 0.3, 0.5) W (light to dark red). In-trap atom numbers for Li $N^{(\text{Li})}$ are given on the left vertical axis, and each point is the average of ten experimental runs. The extracted lifetimes are found to be power-independent within the experimental uncertainties. For all measurements, the error bars represent the standard error of the mean. The two different measurement settings are sketched in the upper right corner inset.

$k_B \cdot 250 \text{ nK/s}$. Normalizing these numbers to the dimple trap depth for Li, we obtain $\gamma^{(\text{Er})}/U^{(\text{Li})} = 8 \text{ mHz}/\mu\text{K } k_B$ or $\dot{E}^{(\text{Er})}/U^{(\text{Li})} = 1.3 \text{ nK}/\mu\text{K s}$. The geometric overlap of the Er cloud and dimple beam is only 6%, leading to an effective heating rate of $\dot{E}_{\text{eff}}^{(\text{Er})} = k_B \cdot 15 \text{ nK/s}$. These calculations are based on the Er line data published in [31] with the theory data replaced by the experimental values for the lines at 401 nm, 583 nm and 841 nm [50–52].

We also measure the dissipative effects of the dimple on Li trapped in it. To this end, we prepare Li in a balanced $|F, m_F\rangle = |1/2, 1/2\rangle, |3/2, -3/2\rangle$ hyperfine state mixture and measure its lifetime for different dimple trap powers (see Fig. 2). We observe a power-independent $1/e$ -lifetime with a mean value of $\tau_{841}^{(\text{Li})} = 14.6 \pm 0.4 \text{ s}$. The power independence (also observed for Er and Li in the 1064 nm trap) suggests that we reach the fundamental limit given by photon scattering, for which the imparted energy and trap depth both scale linearly with the laser intensity. The off-resonant scattering for Li is dominated by its 671 nm line, which is $\Delta_{671}^{(\text{Li})} \approx 1.5 \cdot 10^7 \Gamma_{671}^{(\text{Li})}$ detuned. The photon scattering rate is the same as for Er: $\gamma^{(\text{Li})}/U^{(\text{Li})} = 8 \text{ mHz}/\mu\text{K } k_B$, but the energy input rate is 28-fold increased to $\dot{E}^{(\text{Li})}/U^{(\text{Li})} = 40 \text{ nK}/\mu\text{K s}$ due to the smaller mass. It is important to note that the energy input rate is not always the relevant number. For small sample sizes of about 100 atoms, the timescale provided

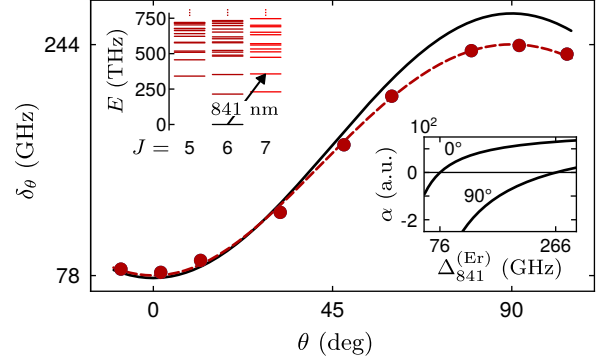


Figure 3. Polarization dependence of the tune-out wavelength. Measured tune-out frequencies (red dots) are given as detuning from the 841 nm-line for different angles between the linear polarization θ and the magnetic field. The tune-out frequencies δ_θ change sinusoidally in dependence of θ in an interval of 166 GHz. The contributing lines up to 400 nm are visualized in the energy level diagram (inset, top left), where the lines connecting to the dark red states cause the θ -dependence. The inset on the bottom right displays the calculated polarizability for parallel and perpendicular polarized linear light, visualizing the shift of the zero-crossing/tune-out point for the two extreme configurations. While the theory (black line) matches the measurements for small angles, a significant deviation becomes apparent closer to perpendicular alignment of polarization and magnetic field. We use a fit (dashed blue line) to quantify the origin of this deviation, as detailed in the main text.

by γ can be long enough to perform experiments without any photon scattering.

The tune-out wavelength is expected to show a strong dependence on the polarization angle θ between the linearly polarized light and the magnetic field [31, 53], which has been studied in Dy [27]. This is due to the tensor polarizability of the lanthanides and, in Er, due to the sizable contribution to the tensor polarizability from lines connecting to states with electronic angular momentum differing from $J' = 7$, the value for the 841 nm-line. The most important ones are the broad $J' = 5, 6$ lines in the blue part of the spectrum, and with θ the coupling strength to these lines varies. To measure the polarization dependence, we change θ and repeat the measurement process described above (see Fig. 3). We concentrate on linear polarization, thus, eliminating the effect of the vector light shift [54, 55] and observe a sinusoidal shift of the tune-out frequency between $\delta_{0^\circ} = 78 \text{ GHz}$ and $\delta_{90^\circ} = 244 \text{ GHz}$. A comparison of our measurements with the theoretical prediction, based on the same modified line data set as above, reveals a discrepancy in the amplitude of the θ dependent modulation. We note that the unmodified line data of [31] cannot be matched with our measurements. To quantify the theory-experiment mismatch, we fix the contributions of the well characterized 841 nm-line to the prediction of the scalar

($\alpha_{s,841}$) and tensor ($\alpha_{t,841}$) polarizability. We then decompose the polarizabilities into contributions from this close-by line and all other far-detuned lines by writing $\alpha_s = \alpha_{s,841}/\Delta + \alpha_{s,0}$ and $\alpha_t = \alpha_{t,841}/\Delta + \alpha_{t,0}$ with the far-detuned “background” contributions being constant over the explored frequency interval. We formulate the tune-out condition as $\delta_\theta = -(\alpha_{s,841} + \frac{1}{2}[3\cos^2(\theta) - 1]\alpha_{t,841})/(\alpha_{s,0} + \frac{1}{2}[3\cos^2(\theta) - 1]\alpha_{t,0})$. Fitting this equation to our measurement, results in $\alpha_{s,0} = (193 \pm 5)$ a.u. and $\alpha_{t,0} = (-16 \pm 0.4)$ a.u., with 1 a.u. = $4\pi\epsilon_0 a_b^3$ expressed in the Bohr radius a_b and the vacuum electric permittivity ϵ_0 . The error is dominated by the uncertainty of the line width $\Gamma_{841}^{(\text{Er})} = (8.0 \pm 0.2)$ kHz [52]. Comparing the fitted background polarizabilities to the theoretical prediction $\alpha_{s,0}^{th} = 184$ a.u. reveals little relative difference for the scalar part, but a 10-fold difference in the tensor part $\alpha_{t,0}^{th} = -1.5$ a.u..

We have demonstrated a dissipationless tune-out wavelength for Er, which at the same time allows far-detuned conservative trapping of Li. Our results demonstrate a reduction of the dissipative effects of a tune-out wavelength by one order of magnitude compared to previously realized quantum gas mixtures [28]. This is an important milestone en route to precision control of heteronuclear quantum gas mixtures at the coldest possible temperatures. The combination of Er with Li is very flexible for the future. It allows realizing heavy-light boson-fermion, boson-boson and fermion-boson systems with tunable interactions, of which the Bose-Bose mixture recently has been brought to degeneracy [48]. Er features an even narrower transition line at 1299 nm [56], to which our idea can also be applied. This would result in a further reduction of the dissipation by more than one order of magnitude.

Acknowledgments

We acknowledge funding from the Horizon Europe program HORIZON-CL4-2022-QUANTUM-02-SGA via the project 101113690 (PASQuanS2.1), the Federal Ministry of Education and Research Germany (BMBF) via the project FermiQP (13N15889), the Deutsche Forschungsgemeinschaft within the research unit FOR5522 (Grant No. 499180199) and the Alfried Krupp von Bohlen and Halbach foundation.

Data availability

All data presented in this manuscript is available from the authors upon reasonable request.

* These authors contributed equally to this work.

† christian.gross@uni-tuebingen.de

- [1] C. Baroni, G. Lamporesi, and M. Zaccanti, Quantum mixtures of ultracold gases of neutral atoms, *Nat Rev Phys* **6**, 736 (2024).
- [2] S. L. Cornish, M. R. Tarbutt, and K. R. A. Hazzard, Quantum computation and quantum simulation with ul-

- tracold molecules, *Nat. Phys.* **20**, 730 (2024).
- [3] T. Langen, G. Valtolina, D. Wang, and J. Ye, Quantum state manipulation and cooling of ultracold molecules, *Nat. Phys.* **20**, 702 (2024).
- [4] F. Scazza, M. Zaccanti, P. Massignan, M. M. Parish, and J. Levinsen, Repulsive Fermi and Bose Polarons in Quantum Gases, *Atoms* **10**, 55 (2022).
- [5] F. Grusdt, N. Mostaan, E. Demler, and L. A. Peña Ardila, Impurities and polarons in bosonic quantum gases: a review on recent progress, *Rep. Prog. Phys.* 10.1088/1361-6633/add94b (2025).
- [6] P. Naidon and S. Endo, Efimov physics: A review, *Rep. Prog. Phys.* **80**, 056001 (2017).
- [7] B. J. DeSalvo, K. Patel, G. Cai, and C. Chin, Observation of fermion-mediated interactions between bosonic atoms, *Nature* **568**, 61 (2019).
- [8] C. Baroni, B. Huang, I. Fritsche, E. Dobler, G. Anich, E. Kirilov, R. Grimm, M. A. Bastarrachea-Magnani, P. Massignan, and G. M. Bruun, Mediated interactions between Fermi polarons and the role of impurity quantum statistics, *Nat. Phys.* **20**, 68 (2024).
- [9] G. Cai, H. Ando, S. McCusker, and C. Chin, Fermion mediated pairing in the Ruderman-Kittel-Kasuya-Yosida to Efimov transition regime, arXiv:2502.06266 .
- [10] L. J. LeBlanc and J. H. Thywissen, Species-specific optical lattices, *Phys. Rev. A* **75**, 053612 (2007).
- [11] J. Catani, G. Barontini, G. Lamporesi, F. Rabatti, G. Thalhammer, F. Minardi, S. Stringari, and M. Inguscio, Entropy Exchange in a Mixture of Ultracold Atoms, *Phys. Rev. Lett.* **103**, 140401 (2009).
- [12] E. Copenhaver, K. Cassella, R. Berghaus, and H. Müller, Measurement of a ^7Li tune-out wavelength by phase-patterned atom interferometry, *Phys. Rev. A* **100**, 063603 (2019).
- [13] B. Décamps, J. Vigué, A. Gauguet, and M. Büchner, Measurement of the 671-nm tune-out wavelength of ^7Li by atom interferometry, *Phys. Rev. A* **101**, 033614 (2020).
- [14] W. F. Holmgren, R. Trubko, I. Hromada, and A. D. Cronin, Measurement of a Wavelength of Light for Which the Energy Shift for an Atom Vanishes, *Phys. Rev. Lett.* **109**, 243004 (2012).
- [15] D. C. McKay, C. Meldgin, D. Chen, and B. DeMarco, Slow Thermalization between a Lattice and Free Bose Gas, *Phys. Rev. Lett.* **111**, 063002 (2013).
- [16] R. Trubko, M. D. Gregoire, W. F. Holmgren, and A. D. Cronin, Potassium tune-out-wavelength measurement using atom interferometry and a multipass optical cavity, *Phys. Rev. A* **95**, 052507 (2017).
- [17] B. Arora, M. S. Safronova, and C. W. Clark, Tune-out wavelengths of alkali-metal atoms and their applications, *Phys. Rev. A* **84**, 043401 (2011).
- [18] C. D. Herold, V. D. Vaidya, X. Li, S. L. Rolston, J. V. Porto, and M. S. Safronova, Precision Measurement of Transition Matrix Elements via Light Shift Cancellation, *Phys. Rev. Lett.* **109**, 243003 (2012).
- [19] R. H. Leonard, A. J. Fallon, C. A. Sackett, and M. S. Safronova, High-precision measurements of the ^{87}Rb D-line tune-out wavelength, *Phys. Rev. A* **92**, 052501 (2015).
- [20] F. Schmidt, D. Mayer, M. Hohmann, T. Lausch, F. Kindermann, and A. Widera, Precision measurement of the ^{87}Rb tune-out wavelength in the hyperfine ground state $F = 1$ at 790 nm, *Phys. Rev. A* **93**, 022507 (2016).

- [21] A. Rubio-Abadal, J.-y. Choi, J. Zeiher, S. Hollerith, J. Rui, I. Bloch, and C. Gross, Many-Body Delocalization in the Presence of a Quantum Bath, *Phys. Rev. X* **9**, 041014 (2019).
- [22] A. Ratkuta, P. D. Gregory, A. D. Innes, A. J. Matthies, L. A. McArd, J. M. Mortlock, M. S. Safronova, S. L. Bromley, and S. L. Cornish, Measurement of the tune-out wavelength for ^{133}Cs at 880nm, *Phys. Rev. A* **104**, 052813 (2021).
- [23] B. Henson, R. Khakimov, R. Dall, K. Baldwin, L.-Y. Tang, and A. Truscott, Precision Measurement for Metastable Helium Atoms of the 413nm Tune-Out Wavelength at Which the Atomic Polarizability Vanishes, *Phys. Rev. Lett.* **115**, 043004 (2015).
- [24] A. Heinz, A. Park, N. Šantić, J. Trautmann, S. Porsev, M. Safronova, I. Bloch, and S. Blatt, State-Dependent Optical Lattices for the Strontium Optical Qubit, *Phys. Rev. Lett.* **124**, 203201 (2020).
- [25] T. O. Höhn, E. Staub, G. Brochier, N. Darkwah Oppong, and M. Aidelburger, State-dependent potentials for the $^1\text{S}_0$ and $^3\text{P}_0$ clock states of neutral ytterbium atoms, *Phys. Rev. A* **108**, 053325 (2023).
- [26] T. O. Höhn, R. A. Villela, E. Zu, L. Bezzo, R. M. Kroeze, and M. Aidelburger, Determining the $^3\text{P}_0$ excited-state tune-out wavelength of ^{174}Yb in a triple-magic lattice, *arXiv:2412.14163*.
- [27] W. Kao, Y. Tang, N. Q. Burdick, and B. L. Lev, Anisotropic dependence of tune-out wavelength near Dy 741-nm transition, *Opt. Express* **25**, 3411 (2017).
- [28] V. D. Vaidya, J. Tiamsuphat, S. L. Rolston, and J. V. Porto, Degenerate Bose-Fermi Mixtures of Rubidium and Ytterbium, *Phys. Rev. A* **92**, 043604 (2015).
- [29] T. Hewitt, T. Bertheas, M. Jain, Y. Nishida, and G. Barontini, Controlling the interactions in a cold atom quantum impurity system, *Quantum Sci. Technol.* **9**, 035039 (2024).
- [30] E. Lippi, M. Gerken, S. Häfner, M. Repp, R. Pires, M. Rautenberg, T. Krom, E. D. Kuhnle, B. Tran, J. Ullmanis, B. Zhu, L. Chomaz, and M. Weidemüller, An Experimental Platform for Studying the Heteronuclear Efimov Effect with an Ultracold Mixture of ^6Li and ^{133}Cs Atoms, *Few-Body Syst* **66**, 1 (2024).
- [31] J. H. Becher, S. Baier, K. Aikawa, M. Lepers, J.-F. Wyart, O. Dulieu, and F. Ferlaino, Anisotropic polarizability of erbium atoms, *Phys. Rev. A* **97**, 012509 (2018).
- [32] A. Christianen, J. I. Cirac, and R. Schmidt, Chemistry of a Light Impurity in a Bose-Einstein Condensate, *Phys. Rev. Lett.* **128**, 183401 (2022).
- [33] R. Onofrio and C. Presilla, Reaching Fermi Degeneracy in Two-Species Optical Dipole Traps, *Phys. Rev. Lett.* **89**, 100401 (2002).
- [34] C. Presilla and R. Onofrio, Cooling Dynamics of Ultracold Two-Species Fermi-Bose Mixtures, *Phys. Rev. Lett.* **90**, 030404 (2003).
- [35] A. Griessner, A. J. Daley, S. R. Clark, D. Jaksch, and P. Zoller, Dark-State Cooling of Atoms by Superfluid Immersion, *Phys. Rev. Lett.* **97**, 220403 (2006).
- [36] M. Bruderer, A. Klein, S. R. Clark, and D. Jaksch, Transport of Strong-Coupling Polarons in Optical Lattices, *New J. Phys.* **10**, 033015 (2008).
- [37] A. J. Matthies, J. M. Mortlock, L. A. McArd, A. P. Raghuram, A. D. Innes, P. D. Gregory, S. L. Bromley, and S. L. Cornish, Long-distance optical-conveyor-belt transport of ultracold ^{133}Cs and ^{87}Rb atoms, *Phys. Rev. A* **109**, 023321 (2024).
- [38] See Supplemental Material at URL for a more detailed description of the production of Er and Li gases which includes [39–42], presentation and discussion of the polarizability calculations, considerations of the lifetime in a red-detuned optical dipole trap and Er lines used for the polarizability calculations.
- [39] K. Aikawa, A. Frisch, M. Mark, S. Baier, A. Rietzler, R. Grimm, and F. Ferlaino, Bose-Einstein Condensation of Erbium, *Phys. Rev. Lett.* **108**, 210401 (2012).
- [40] G. A. Phelps, A. Hébert, A. Krahn, S. Dickerson, F. Öztürk, S. Ebadi, L. Su, and M. Greiner, Sub-second production of a quantum degenerate gas, *arXiv:2007.10807*.
- [41] W. Lunden, L. Du, M. Cantara, P. Barral, A. O. Jamison, and W. Ketterle, Enhancing the capture velocity of a Dy magneto-optical trap with two-stage slowing, *Phys. Rev. A* **101**, 063403 (2020).
- [42] B. Plotkin-Swing, A. Wirth, D. Gochner, T. Rahman, K. E. McAlpine, and S. Gupta, Crossed-beam slowing to enhance narrow-line ytterbium magneto-optic traps, *Rev. Sci. Instrum.* **91**, 093201 (2020).
- [43] G. Zürn, T. Lompe, A. Wenz, S. Jochim, P. Julienne, and J. Hutson, Precise Characterization of ^6Li Feshbach Resonances Using Trap-Sideband-Resolved RF Spectroscopy of Weakly Bound Molecules, *Phys. Rev. Lett.* **110**, 135301 (2013).
- [44] A. Frisch, M. Mark, K. Aikawa, F. Ferlaino, J. L. Bohn, C. Makrides, A. Petrov, and S. Kotochigova, Quantum chaos in ultracold collisions of gas-phase erbium atoms, *Nature* **507**, 475 (2014).
- [45] F. Schäfer, N. Mizukami, and Y. Takahashi, Feshbach Resonances of Large-Mass-Imbalance Er-Li Mixtures, *Phys. Rev. A* **105**, 012816 (2022).
- [46] C. Presilla and R. Onofrio, Cooling Dynamics of Ultracold Two-Species Fermi-Bose Mixtures, *Phys. Rev. Lett.* **90**, 030404 (2003).
- [47] K. Xie, X. Li, Y.-Y. Zhou, J.-H. Luo, S. Wang, Y.-Z. Nie, H.-C. Shen, Y.-A. Chen, X.-C. Yao, and J.-W. Pan, Feshbach spectroscopy of ultracold mixtures of ^6Li and ^{164}Dy atoms, *arXiv:2502.08099*.
- [48] J. Kalia, J. Rivera, R. R. Emran, W. J. S. Hernandez, K. Kwon, and R. J. Fletcher, Creation of a Degenerate Bose-Bose Mixture of erbium and lithium atoms, *arXiv:2506.00177*.
- [49] P. Barakhshan, A. Marrs, A. Bhosale, B. Arora, R. Eigenmann, and M. S. Safronova, Portal for High-Precision Atomic Data and Computation (version 2.0). University of Delaware, Newark, DE, USA. URL: <https://www.udel.edu/atom>.
- [50] A. Frisch, K. Aikawa, M. Mark, F. Ferlaino, E. Berseneva, and S. Kotochigova, Hyperfine structure of laser-cooling transitions in fermionic erbium-167, *Phys. Rev. A* **88**, 032508 (2013).
- [51] E. A. D. Hartog, J. P. Chisholm, and J. E. Lawler, Radiative lifetimes of neutral erbium, *J. Phys. B: At. Mol. Opt. Phys.* **43**, 155004 (2010).
- [52] H. Y. Ban, M. Jacka, J. L. Hanssen, J. Reader, and J. J. McClelland, Laser cooling transitions in atomic erbium, *Opt. Express* **13**, 3185 (2005).
- [53] M. Lepers, J.-F. Wyart, and O. Dulieu, Anisotropic optical trapping of ultracold erbium atoms, *Phys. Rev. A* **89**, 022505 (2014).

- [54] F. Le Kien, P. Schneeweiss, and A. Rauschenbeutel, Dynamical polarizability of atoms in arbitrary light fields: general theory and application to cesium, *Eur. Phys. J.* **67**, 92 (2013).
- [55] H. Li, J.-F. Wyart, O. Dulieu, and M. Lepers, Anisotropic optical trapping as a manifestation of the complex electronic structure of ultracold lanthanide atoms: The example of holmium, *Phys. Rev. A* **95**, 062508 (2017).
- [56] A. Patscheider, B. Yang, G. Natale, D. Petter, L. Chomaz, M. J. Mark, G. Hovhannesian, M. Lepers, and F. Ferlaino, Observation of a narrow inner-shell orbital transition in atomic erbium at 1299 nm, *Phys. Rev. Res.* **3**, 033256 (2021).
- [57] W. I. McAlexander, E. R. I. Abraham, and R. G. Hulet, Radiative lifetime of the $2P$ state of lithium, *Phys. Rev. A* **54**, R5 (1996).

Supplementary Material

This supplementary file provides background information about the experimental sequence and the theoretical calculations underlying our manuscript.

Experimental sequence

For the characterization of the tune-out for Er, our experiments start with the preparation of the trapped Er cloud. The procedure follows the standard approach for this atom [39, 40]. We use a spin-flip Zeeman slower on the strong line of Er at 401 nm ($\Gamma = 2\pi \cdot 29.7$ MHz), which is directly loading a narrow-line magneto-optical trap (MOT) at 583 nm ($\Gamma = 2\pi \cdot 190$ kHz). An important addition to this setup was the use of “angled slowing” beams [41, 42]. Two beams, red-detuned from the 401 nm-transition, were aligned to cross just before the MOT region and provide an intermediate slowing step, after the slower’s exit and right in front of the MOT’s capture region. In our setup, this additional cooling improved the MOT loading rate by more than an order of magnitude, reaching $4 \cdot 10^7$ /s. After a loading time of 5 s, the compressed MOT (cMOT) contains a approximately $2 \cdot 10^8$ atoms, cooled down to $8 \mu\text{K}$ and optically pumped into the lowest Zeeman state $|J, m_J\rangle = |6, -6\rangle$.

The atoms are then transferred from the cMOT into a crossed-beam optical dipole trap (ODT), consisting of two laser beams at 1064 nm, focused to a waist of $80 \mu\text{m}$ at 30 W each. To this trap, an additional beam used later for transport is superimposed, also at 1064 nm and with a e^{-2} radius of $500 \mu\text{m}$ at 80 W. To transport this cloud into the glass cell, we ramp up a second transport beam to 30 W to create a horizontal lattice. To transport this cloud into the glass cell, we ramp up a second transport beam to 30 W to create a horizontal lattice. We then ramp down the ODT power and move the lattice over 0.5 m in 165 ms by detuning one of the lattice beams. However, this lattice is not strong enough to hold the Er atoms against gravity, and we use two elongated coils (“racetrack coils”) to generate a vertical magnetic field gradient of 4.2 G/cm at a vertical offset field of 22 G. This levitates the cloud over the entire transport distance. Finally, the cloud is transferred in an elliptical ODT consisting of two laser beams of vertical and horizontal waists of $(\omega_v, \omega_h) = (35, 580) \mu\text{m}$, at 1064 nm and 10 W each. The vertical confinement is strong enough to switch off the levitation field, while the vertical offset field is reduced to 4.9 G.

The production of an ultra-cold gas of Li and its transport to the glass cell follows similar steps as for Er. We start with a MOT loaded from a decreasing-field Zeeman slower, both working on the D_2 -line at 671 nm ($\Gamma = 2\pi \cdot 5.9$ MHz [57]). An important, non-standard feature of our setup is the implementation of a trans-

verse cooling and optical pumping stage before the Zeeman slower input. By using a two-dimensional molasses on the D_1 -line, the atoms are pumped into the hyperfine $|F, m_F\rangle = |3/2, -3/2\rangle$ state, which is the only one being addressed by the Zeeman slower. The combined contributions of pumping and transversal cooling result in a ten-fold increase in the MOT loading rate, yielding a value of $2 \cdot 10^7$ /s. After a loading time of 5 s, and at the end of a cMOT stage, we measure approximately 10^8 atoms, cooled down to $300 \mu\text{K}$.

The Li cloud is then transferred to a 1070 nm multimode ODT consisting of two horizontal beams overlapped at an angle of 10° , with powers and waists of 150 W and $65 \mu\text{m}$. The Li cloud is in an equal spin mixture of $|F, m_F\rangle = |1/2, \pm 1/2\rangle$. It is further cooled by evaporating at 320 G by ramping down the laser power for 2.4 s. At this stage, we reach degeneracy when evaporating further. Right before the end of evaporation, we ramp up the transport lattice, and transport the atoms over a distance of 1 m into the glass cell. The transport of Li takes 112 ms. When the atoms have arrived in the glass cell, we transfer the population from state $|1/2, -1/2\rangle$ to state $|3/2, -3/2\rangle$. This is being done by a rapid adiabatic passage with a 100 kHz wide sweep of a rf-field over the resonance at 3.4 G in 25 ms. Finally, the cloud is transferred to the same elliptical trap as Er before, and then loaded into the tune-out dimple trap at 841 nm with waists of $(\omega_v, \omega_h) = (6, 28) \mu\text{m}$.

Theory of polarizability / tune-out

When exposed to a light field, an atom gets polarized and its electronic cloud’s distribution is modified. The atom’s response generally depends on its state and dipole-allowed transitions, but also on the wavelength, polarization, and relative orientation of the light to the atom. This interaction results in an energy shift of the atom proportional to the intensity $I = \frac{\epsilon_0 c}{2} |\mathbf{E}|^2$ of the light field. Here \mathbf{E} is the electric field, ϵ_0 the vacuum permittivity and c the speed of light. Suppose linear polarized light, the angle between the polarization and the quantization axis (usually given by an offset magnetic field) is denoted by the angle θ and the angle between the propagation of the light field and the quantization axis is denoted by κ . The total polarizability α_{tot} of an atom and its energy shift can be decomposed into three

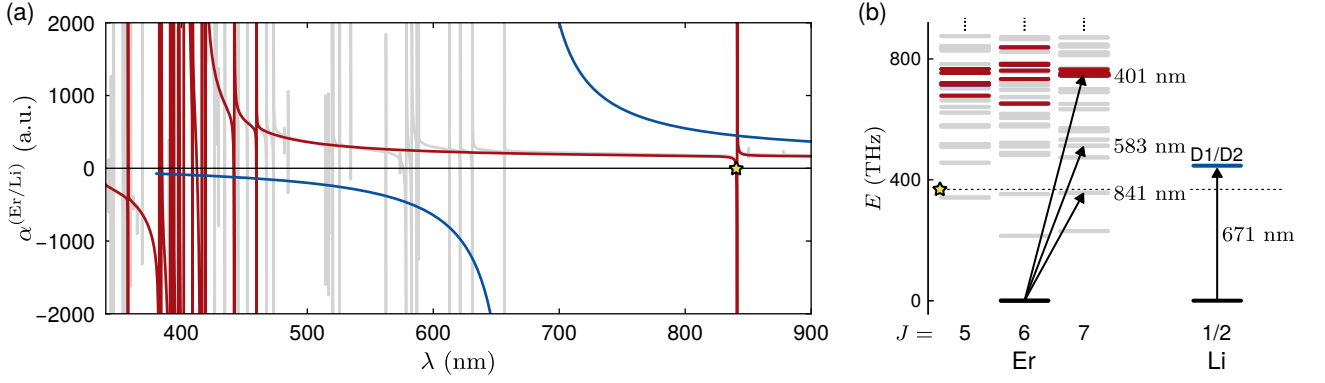


Figure 4. (a) Polarizabilities of Er and Li, with the relevant tune-out highlighted (star). The total polarizability of Er (gray) consists of contributions from many lines, but it is dominated by strong lines in the blue and UV. Those lines together with the 841 nm line (red) govern the position of the tune-out wavelength, which is blue detuned from this $2\pi \times 8$ kHz narrow line. The polarizability of Li (blue) is dominated by the 671 nm D₁ and D₂ lines. The tune-out point near 841 nm of Er is far red-detuned to them, which allows creating attractive optical dipole traps for Li at that wavelength. (b) Energy levels for Er and Li. Arrows indicate commonly used cooling transitions. Strong and weak Er lines are colored the same way as in (a).

contributions [55] of distinct character, respectively:

$$\begin{aligned}
 U(\omega) &= -\frac{1}{2\epsilon_0 c} I(r) \alpha_{tot} \\
 &= -\frac{1}{2\epsilon_0 c} I(r) \left[\alpha_s(\omega) + |\mathbf{u}^* \times \mathbf{u}| \cos(\kappa) \frac{m_J}{2J} \alpha_v(\omega) \right. \\
 &\quad \left. + \underbrace{\frac{3m_J^2 - J(J+1)}{J(2J-1)}}_{=1, \forall |m_J| = J \neq 1/2} \frac{3\cos^2(\theta) - 1}{2} \alpha_t(\omega) \right].
 \end{aligned} \tag{1}$$

The scalar contribution $\alpha_s(\omega)$ depends solely on the wavelength of the light, and is the main contributor to the polarizability of alkali atoms. It is the same for all Zeeman substates. The vector contribution $\alpha_v(\omega)$ acts as a fictitious magnetic field. Its impact vanishes for linear polarized fields, as the cross product $|\mathbf{u}^* \times \mathbf{u}| = 0$ of a real polarization vector.

The tensor contribution $\alpha_t(\omega)$ originates from an induced polarization perpendicular to the electric field wave vector of the driving field. It does not contribute to atoms in $J = 1/2$ states, which holds for all alkali ground states. It also vanishes for $\theta_0 = 54.7^\circ$. For alkaline-earth and lanthanide atoms, a more complex electron configuration leads to high ground state total angular momentum numbers of, e.g., $J = 6$ for Er, and thus generally to a non-vanishing contribution of α_t . The three individual contributions are given by:

$$\begin{aligned}
 \alpha_s(\omega) &= -\sqrt{\frac{1}{3(2J+1)}} \alpha_J^{(0)}(\omega), \\
 \alpha_v(\omega) &= +\sqrt{\frac{2J}{(J+1)(2J+1)}} \alpha_J^{(1)}(\omega), \\
 \alpha_t(\omega) &= +\sqrt{\frac{2J(2J-1)}{3(J+1)(2J+1)(2J+3)}} \alpha_J^{(2)}(\omega),
 \end{aligned}$$

with

$$\begin{aligned}
 \alpha_J^{(K)}(\omega) &= \sqrt{2K+1} \times \sum_{J'} (-1)^{J+J'} \\
 &\quad \times \left\{ \begin{matrix} 1 & K & 1 \\ J & J' & J \end{matrix} \right\} |\langle J' || \mathbf{d} || J \rangle|^2 \\
 &\quad \times \frac{1}{\hbar} \text{Re} \left[\frac{1}{\Delta_{J',J}^- - i\gamma_{J',J}/2} + \frac{(-1)^K}{\Delta_{J',J}^+ - i\gamma_{J',J}/2} \right].
 \end{aligned}$$

The sum includes all dipole allowed transitions from J to J' ($\Delta J = \pm 1, 0$). The curly brackets matrix denotes the Wigner 6-j symbol. We calculate the reduced dipole transition element $|\langle J' || \mathbf{d} || J \rangle|$ as in [54]. $\gamma_{J'}$ is the excited state natural line width and $\Delta_{J',J}^\pm = \omega_{J',J} \pm \omega$.

Our calculations are based on the theoretical line data provided in [31], which we modified with experimentally measured values for the lines 841 nm [52], 583 nm [51] and 401 nm [50]. In the following, we assume that the light travels perpendicular to the magnetic field ($\kappa = 90^\circ$), which leaves us with only the scalar and tensor contributions of Eq. (1). We take the polarizability of Li from [49] and display the Er and Li polarizabilities together in Fig. 4. The isolation of the 841 nm line from the strong lines in the blue is apparent. On the tune-out point of Er, the Li 671 nm lines are far red-detuned leading to an attractive optical potential.